Laser-Induced Transient Anisotropy and Large Amplitude Magnetization Dynamics in a Gd/FeCo Multilayer

Document status and date:
Published: 20/12/2022

Document Version:
Publisher's PDF, also known as Version of Record (includes final page, issue and volume numbers)

Please check the document version of this publication:

• A submitted manuscript is the version of the article upon submission and before peer-review. There can be important differences between the submitted version and the official published version of record. People interested in the research are advised to contact the author for the final version of the publication, or visit the DOI to the publisher's website.
• The final author version and the galley proof are versions of the publication after peer review.
• The final published version features the final layout of the paper including the volume, issue and page numbers.

[Link to publication](#)

Laser-Induced Transient Anisotropy and Large Amplitude Magnetization Dynamics in a Gd/FeCo Multilayer

Thomas G.H. Blank, Sten Hermanussen, Tom Lichtenberg, Theo Rasing, Andrei Kirilyuk, Bert Koopmans, and Alexey V. Kimel*

Ultrafast laser-induced dynamics in a ferrimagnetic gadolinium iron cobalt (Gd/FeCo) multilayer with a magnetization compensation temperature of $T_M = 320$ K is studied at room temperature as a function of laser-fluence and strength of the applied magnetic field. The dynamics is found to be substantially different from that in archetypical GdFeCo alloys, and depending on the laser fluence one can distinguish two different regimes. At low laser fluence ($\lesssim$1.6 mJ cm^{-2}), ultrafast laser excitation of the medium triggers spin precession of an extraordinary large amplitude reaching over 30°. At high laser fluence ($\geqslant$2.2 mJ cm^{-2}), the pump heats the medium over the magnetization compensation point, spin precession reduces significantly in amplitude and the process of field-assisted reversal of magnetization of Gd and FeCo is launched. It is argued that such a distinctly different laser-induced magnetization dynamics in the multilayers compared to the alloys is due to the symmetry breaking at the numerous interfaces, giving rise to additional surface anisotropy. The temperature dependence of the latter is found to be the key ingredient in the mechanism of ultrafast laser-induced magnetization dynamics in ferrimagnetic multilayers. Controlling the amount and properties of interfaces in multilayers can thus serve as a mean to achieve efficient ultrafast all-optical control of magnetism.

1. Introduction

The ability to control the magnetization of magnetically ordered media with the help of femtosecond laser pulses opened up new perspectives for data storage technologies as well as motivated an intense research interest to fundamentally new, ultrafast, and

T. G. H. Blank, S. Hermanussen, Th. Rasing, A. V. Kimel
Institute for Molecules and Materials
Radboud University
Nijmegen 6525 AJ, The Netherlands
E-mail: a.kimel@science.ru.nl
T. G. H. Blank, T. Lichtenberg, B. Koopmans
Department of Applied Physics
Eindhoven University of Technology
P.O. Box 513, Eindhoven 5600 MB, The Netherlands
A. Kirilyuk
FELIX Laboratory
Radboud University
Nijmegen 6525 ED, The Netherlands

least dissipative mechanisms to influence magnetization with the help of light.[1] Ferrimagnetic materials, in this respect, have shown so far the most dramatic response to ultrafast laser excitation, starting with the observation of the switching of the magnetization in the metallic ferrimagnetic alloy GdFeCo with a single 40 femtosecond laser pulse.[2] This mechanism was demonstrated to proceed via a strongly non-equilibrium transient ferromagnetic phase [3] as a result of laser-induced heating.[4] Later, a non-thermal mechanism of optical recording of magnetic bits was achieved in a dielectric ferrimagnet via photo-induced changes of the magnetic anisotropy.[5] More recently, it was shown that such a ferrimagnetic dielectrics also facilitate a novel mechanism of heat-assisted magnetic recording (HAMR),[6,7] which does not require nearly complete demagnetization like in GdFeCo, but relies on the temperature dependence of the magnetic anisotropy.[8] This rises the question whether ultrafast changes in magnetic anisotropy could also play a role in metallic ferrimagnets. However, despite intense research interest in metallic ferrimagnets, magnetization dynamics and eventual magnetic switching as a result of ultrafast dynamics of magnetic anisotropy has not been discussed yet.

Here, in order to study the role of the temperature dependence of the magnetic anisotropy in laser-induced magnetization dynamics of metallic ferrimagnets, we consider a ferrimagnetic Gd/FeCo multilayer. In the past few years, laser-induced phenomena of rare-earth transition-metal (RE-TM) multilayer heterostructures have been investigated and compared to alloys, focusing mainly on all-optical switching.[9–13] In this context, the biggest difference of multilayers compared to alloys is the weaker effective antiferromagnetic exchange interaction between the rare-earth and transition-metal spins as a consequence of the reduced RE-TM contact area that is being restricted to the interfaces. A lesser exposed aspect is the effect of structural anisotropy, caused by the arrangement of an isotropic alloy in layers, on the magnetic anisotropy. That is, as the symmetry is broken at the interfaces, the structure could gain additional and controllable contributions to the magnetic anisotropy.[14,15] By performing pump–probe magneto–optical measurements as a function of magnetic field and pump-fluence, we show that the laser-induced dynamics in our multilayer is dramatically different from that known for

ADVANCED
SCIENCE NEWS
www.advancedsciencenews.com

ADVANCED
MATERIALS
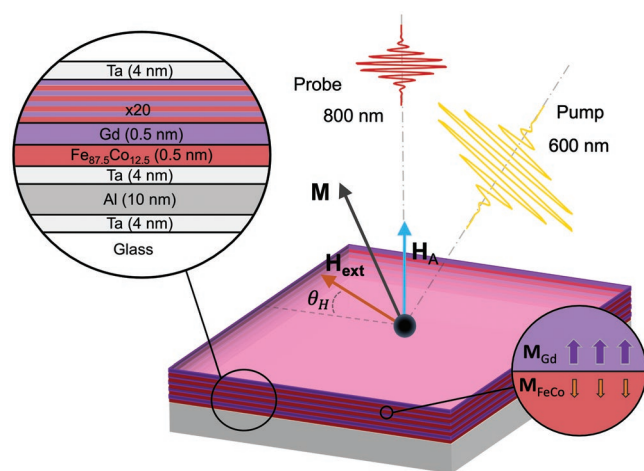**INTERFACES**
www.advmatinterfaces.de

Figure 1. Schematic of the multilayer structure and pump–probe experiment. In macro-spin approximation, this sample consists of two antiferromagnetically coupled macroscopic magnetic sublattices M_{Gd} and M_{Fe} corresponding to the sum of the magnetic moments of the Gd and FeCo layers, respectively. An external magnetic field $\mu_0|H_{ext}|$ of at most 320 mT applied at an angle of $\theta_H \approx 11°$ tilts the net magnetic moment $M \equiv M_{Gd} + M_{Fe}$ along the field away from the easy (z-)axis of anisotropy.

the alloys. The results indicate that laser-induced dynamics of the magnetic anisotropy plays a dominant role in the observed magnetization dynamics.

2. Experimental Section

Previous results obtained on $Gd_xFe_{100–x–y}Co_y$ alloys showed that compositions with $22 \leqslant x \leqslant 26$ and $9.3 \leqslant y \leqslant 9.8$ were characterized by the strongest magnetic response to ultrafast laser excitation.[16] Therefore, a multilayer consisting of 20 alternating Gd (0.5 nm) and $Fe_{87.5}Co_{12.5}$ (0.5 nm) layers was studied. Considering the unit volume occupied by the Gd, Fe, and Co atoms determined by the corresponding metallic radii $r_{Gd} = 1.8$ Å, $r_{Fe} = 1.26$ Å, and $r_{Co} = 1.25$ Å,[17,18] such a synthetic heterostructure is equivalent to the $Gd_{25.5}Fe_{65}Co_{9.5}$ alloy in terms of the number of atoms. The sample stack as schematically illustrated in **Figure 1** was deposited on a glass substrate by magnetron sputtering. The first Ta layer ensured a good attachment of the Al heat-sink, which was shielded from the magnetic [Gd/FeCo] part of the sample by another Ta(4) layer. Afterward, the 20 nm thick magnetic multilayer was capped by a 4 nm Ta layer to prevent it from oxidation. SQUID magnetometry and magneto–optical (MO) characterization of the sample showed that it had perpendicular magnetic anisotropy (PMA), with relatively weak coercive field in the order of about $\mu_0H_c = 10$ mT (see Supporting Information). Similar to the alloy, antiferromagnetic exchange coupling was obtained between the gadolinium (Gd) and transition-metal (FeCo) spins at the interfaces. Moreover, as a consequence of the relatively large magnetic moment and low Curie temperature of Gd compared to FeCo, the sample should exhibit a temperature of magnetization compensation T_M where the net magnetic moment $M(T) = M_{Gd}(T) + M_{Fe}(T)$ is zero. Indeed, MO Faraday effect and SQUID measurements as a function of temperature confirmed a compensation temperature slightly above room temperature $T_M \approx 320$ K (see Supporting Information).

The material was studied in a conventional pump-probe experimental scheme as depicted in Figure 1. In the experiment, the system was excited using an intense and linearly polarized laser pulse with a central wavelength of $\lambda = 600$ nm. The pump pulse approached the sample at near normal incidence being focused in a spot with beam radius $w = 400$ μm. The pump pulses were brought to spatial and temporal overlap with tightly focused (beam radius 50 μm), weak and linearly polarized probe pulses with a central wavelength of $\lambda = 800$ nm. These probe pulses were transmitted at normal incidence through the sample and traveled to a balanced photo-detector. For the pump pulses, a peak fluence $F = 2E_{pulse}/\pi w^2$ up to 5.1 mJ cm^{-2} was used, while the fluence of the probe pulse was many orders of magnitude weaker, such that it did not induce any changes in the medium.

Both pump and probe pulses had a pulse duration of ≈100 fs. The probe pulses were generated at a repetition rate of 1 kHz, but the pump-pulses arrived at the sample at half the rate (500 Hz). The latter frequency was set as a reference to a set of lock-in amplifiers to deduce the pump-induced signal in both the difference and sum channels of the balanced photo-detector. The difference channel measures changes in probe polarization rotation while the sum channel probes changes in probe intensity (transient transmission). It was possible to vary the polarization-angle and intensity of the incoming pump and probe pulses by using half- and quarter-wave plates. An external magnetic field H_{ext} of at most 320 mT that was tilted at an angle $\theta_H \approx 11°$ from the sample plane (see Figure 1) was applied during the measurements. In the following section, the key observations of the pump–probe measurements are presented, performed at room temperature (293 K).

Pump-Probe Experiment: An amplified Ti:Sapphire laser system delivered laser pulses with a central wavelength of $\lambda = 800$ nm at a repetition rate of 1 kHz. The beam was split into two parts: one part served a as probe while the other was sent to a commercial optical parametric amplifier (OPA) to generate pump pulses with a wavelength of 600 nm.

Magneton Sputtering: The Gd/FeCo multilayer used in this experiment was fabricated via magnetron sputtering on a glass substrate for the use of pump–probe experiments in transmission and additionally on a small Si wafer coated with a 100 nm SiO2 layer to use for measurements of magnetic moment in a superconducting quantum interference device vibrating sample magnetometer (SQUID VSM). The base pressure in the deposition chamber was 1.0×10^{-8} mbar. The Fe and Gd targets were connected to a DC voltage source, while a RF voltage was applied to the Co target. In order to obtain a correct ratio of the FeCo alloy, a calibration curve was obtained by growing several alloys for various voltages on the iron target, followed by a determination of the content ratio by comparing the relative amplitudes of the 2p3/2 peaks of iron and cobalt using X-ray photo-electron spectroscopy (XPS), where the X-rays were emitted from an Mg source.

3. Results

Figure 2a shows the hysteresis loop of the polarization rotation of the probe θ_F as a function of external magnetic field, without a

**ADVANCED
SCIENCE NEWS**
www.advancedsciencenews.com
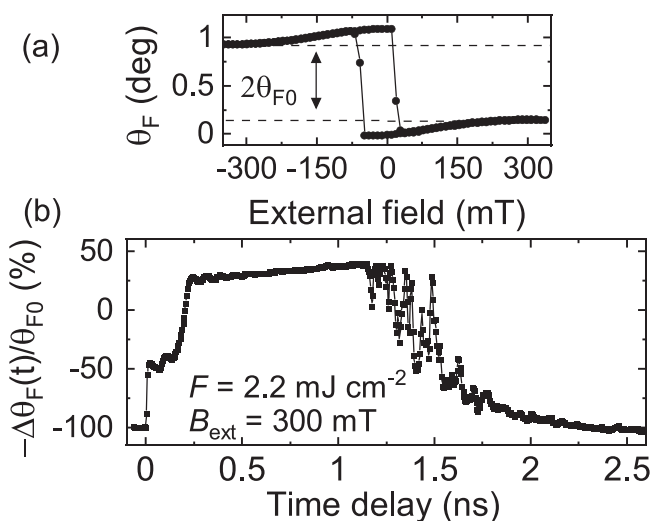
**ADVANCED
MATERIALS
INTERFACES**
www.advmatinterfaces.de

Figure 2. a) Hysteresis loop measured in the experimental scheme described by Figure 1. b) Pump-induced signal at a fluence of $F = 2.2$ mJ cm^{-2} and external magnetic field $B_{ext} = 300$ mT.

pump pulse applied. The contrast $\theta_{F0} = 0.5[\theta_F(+ B_{ext}) - \theta_F(- B_{ext})]$ will throughout be used to normalize the pump-induced polarization rotation changes of the probe. Figure 2b shows a typical transient polarization rotation induced by a pump-pulse at a fluence of $F = 2.2$ mJ cm^{-2}. Within the first picoseconds after the excitation, the polarization rotation $\Delta\theta_F$ decreases steeply, followed by another change of the signal that occurs on a much longer timescale of several hundred picoseconds. Finally, the signal relaxes back to its original value at $t \approx 1.5$ ns that is accompanied by large fluctuations.

Before we proceed with the results, it is crucial to understand the origin of the polarization rotation in this sample. We determined experimentally that both the hysteresis loop and the pump-induced signals are completely independent of probe polarization. Such an independence of probe polarization implies that the detected (transient) changes of θ_F originate from the antisymmetric part of the dielectric permittivity tensor $\varepsilon_{xy}^{(a)} = -\varepsilon_{yx}^{(a)}$.[19] Experimentally, such a polarization rotation is commonly known as the magneto–optical Faraday effect.[1,20] For the present measurement configuration, this effect is exclusively due to changes of the magnetization along the out-of-plane z-axis.[21,22]

Based on the interpretation $\theta_F \propto M_z$, the hysteresis loop in Figure 2a shows that even for the maximal field of $B_{ext} = 300$ mT, the magnetization is predominantly along the z-axis with only a small canting towards the sample plane. Considering the dynamics in Figure 2b, we can now assign the ultrafast change directly after the pulse-excitation to the well-known phenomena of ultrafast demagnetization,[3,23,24] leaving the system in a highly non-equilibrium state with partially (≈50%) quenched magnetization. It is most likely that the temperature of the non-equilibrium state crossed T_M, which then somehow instigates switching of the magnetization on a time-scale of ≈200 ps, similar to what has been reported earlier in the alloy.[25] After the magnetization reversal, the magnetization dynamics exhibits a return at $t \approx 1.5$ ns toward the equilibrium initial state. It is remarkable that the relaxation dynamics in this region is sud-

denly accompanied by strong fluctuations, which in stroboscopic measurements indicates a stochasticity of the process. The exact timing of this relaxation depended on the position of the spot on the sample, and in later measurements, it was not observed within our experimental time-window. We attribute this particular occurrence of a fast back-relaxation to a sample defect, serving as a point of nucleation for this dynamics, but it has not been studied here further. In order to gain a better understanding about what drives the magnetization dynamics in our experiments, we considered the dependencies on pump polarization, fluence, and external magnetic field.

3.1. Polarization, Fluence, and Field Dependence

Our measurements for different pump polarizations revealed that the transient signals are polarization independent. This suggests that the laser-induced dynamics is solely a result of laser-induced heating. The amount of heating is controlled by the pump-fluence and should set the degree of demagnetization of the non-equilibrium state after the first few picoseconds, which in turn should have an impact on the further course of the sub-ns magnetization dynamics. Moreover, the timescale of the sub-ns dynamics corresponds to transverse rather than longitudinal magnetization dynamics (such as ultrafast demagnetization) because the latter is driven by exchange forces and evolves usually on a time-scale of a few picoseconds. The classical theory of transverse magnetization dynamics by Landau and Lifshitz[19] predicts a typical timescale $2\pi(\gamma B)^{-1}$ where B the total effective field and $\gamma/2\pi \approx 28$ GHz T^{-1} if $g = 2$. A dependence on external magnetic field could therefore be expected. Here, we will summarize the experimental dependencies of pump fluence and external magnetic field.

3.1.1. Fluence Dependence

Both the ultrafast sub-ps as well as the sub-ns dynamics are found to be very sensitive to the pump-fluence (see **Figure 3**). It can be seen that a larger fluence results in a larger degree of sub-ps demagnetization. Regarding the subsequent sub-ns dynamics, we discovered various regimes of magnetization dynamics, for low fluence $0.3 \leqslant F \leqslant 1.6$ mJ cm^{-2}, the magnetization oscillates with unusually strong amplitudes. Increasing the fluence to $2.2 \leqslant F \leqslant 3.4$ mJ cm^{-2} suddenly suppresses the oscillations and instead, we observe sub-ns switching of magnetization similar to what we observed in Figure 2. We attribute the sudden suppression of oscillations to the large damping, together with the fact that any precession should occur predominantly along the z-axis that is not picked up by our experiment. When increasing the fluence even further $F \geqslant 4.2$ mJ cm^{-2}, we observe the formation of a plateau. By complementary measurements using single-shot time-resolved magneto–optical microscopy (see Supporting Information), we find that this latter laser-fluence regime leads to a reversal of the magnetization that occurs within a picosecond after the laser pulse excitation. The data in the Supporting Information suggest that this reversal does not depend on field and instead is governed by exchange interaction as is the case for helicity-independent
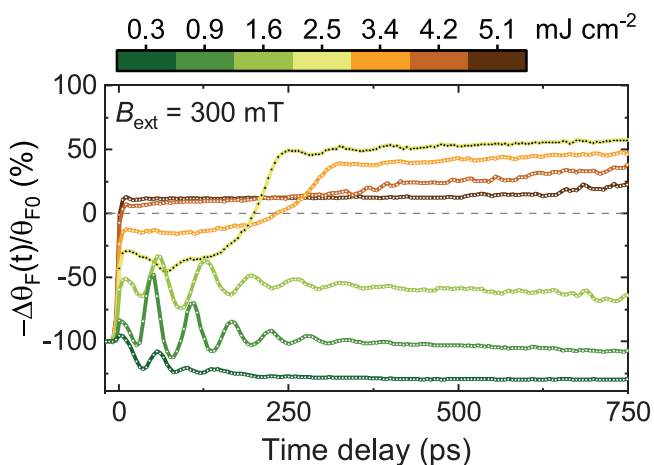
**ADVANCED
SCIENCE NEWS**
www.advancedsciencenews.com

**ADVANCED
MATERIALS
INTERFACES**
www.advmatinterfaces.de

Figure 3. Pump-induced signal as a function of pump-fluence, demonstrating the existence of several regimes. Note that signal at the lowest fluence of 0.3 mJ cm^{-2} drops below 100%, which is possible since the initial magnetization is canted towards the plane by the external magnetic field.

Figure 4. a) Magnetization oscillations for several pump-fluences, measured at an external magnetic field $B_{ext} = 300$ mT. The frequency decreases for increasing fluence. b) Magnetization oscillations where an exponential function associated to thermal demagnetization has been subtracted from the data in order to study the precessional motion only. The fit with constant frequency exposes, although subtle, a mismatch. Instead, the data can be fitted properly when accounting for a linearly increasing frequency of $d\omega/dt \approx 0.17$ GHz period^{-1}.

all-optical-switching (HI-AOS).[4] However, contrary to previous results, the magnetization reversal does not toggle.[3,16] For a more detailed discussion on this high laser-fluence regime, we refer to the Supporting Information. In this article, we only address the first two regimes where $F \leqslant 3.4$ mJ cm^{-2}, and return to the question of the long-timescale dynamics both experimentally and theoretically.

We found the optimal fluence for which the laser triggers magnetization oscillations with the largest amplitude to be ≈ 1.1 mJ cm^{-2} (see **Figure 4**a). In this case, the oscillation amplitude may reach the strikingly large amplitude of 45% of the initial z-component of the magnetization M_{z0} (see Figure 4b). It means that the angle of precession of the net magnetization is at least 30°. Note that in the majority of pump–probe experiments in ultrafast magnetism, an amplitude of magnetization precession of several degrees is considered as large.[26,27] In general, oscillations with large amplitudes imply that modeling the corresponding dynamics would require to go beyond the approximation of a harmonic oscillator. One aspect of anharmonicity is a dependence of the resonance frequency on the amplitude of the oscillations. **Figure 5** shows that the oscillation frequency ω indeed decreases monotonically for increasing laser fluence with ≈ 4.2 GHz/(mJ cm^{-2}), but it scales with fluence rather than with amplitude thus anharmonicity does not seem to be responsible.

Moreover, we discovered that the frequency of the oscillations increases as a function of time delay. In order to illustrate this, we plotted the oscillations at the optimal fluence in Figure 4b, where we subtracted an exponential contribution to the data and therefore extract the precessional waveform. The data cannot be fitted with a harmonic function with constant frequency. Instead, we could fit the data by assuming a linearly time-variable frequency $\omega(t) = \omega_0 + t \cdot \frac{d\omega}{dt}$, demonstrating a chirp of $\frac{d\omega}{dt} \approx 0.17$ GHz period^{-1}. In order to understand the mechanism behind the frequency-dependency on fluence and

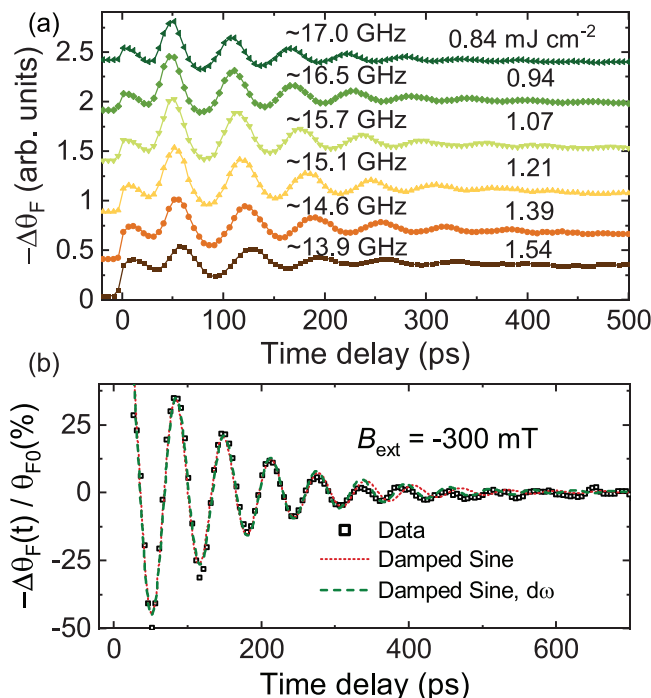time, we have to establish the origin of the magnetization oscillations. For this, we will look at the dynamics as a function of magnetic field.

3.1.2. Field Dependence

Following the classical Landau–Lifshitz theory, the magnetization dynamics should depend on external magnetic field. Indeed, as shown in **Figure 6**a, we observe that the timescale
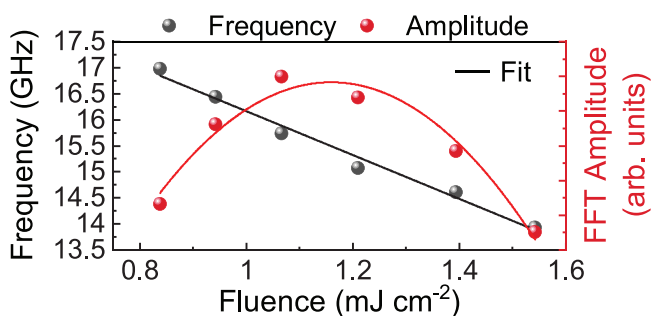

Figure 5. Frequency (black dots) and amplitude (red dots) of the dynamics from Figure 4a plotted as a function of pump fluence. The data suggests there is no one-to-one correspondence between the amplitude and the frequency of the oscillations, implying that the fluence-dependence of the frequency is not due to nonlinearity.
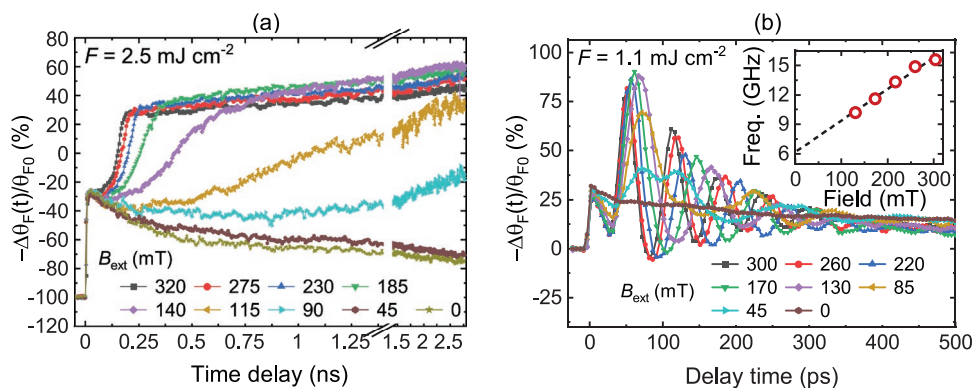
**ADVANCED
SCIENCE NEWS**

www.advancedsciencenews.com

**ADVANCED
MATERIALS
INTERFACES**

www.advmatinterfaces.de

Figure 6. a) Double-step switching process as a function of external field, demonstrating the field-assisted precessional character of the magnetization reversal. b) Magnetization precession measured at the fluence $F = 1.1$ mJ cm^{-2} where the oscillation amplitude is optimal. The inset shows the frequency dependence of the precessional motion as a function of external field.

of magnetization reversal for the fluence region $2.2 \leqslant F \leqslant 3.4$ mJ cm^{-2} has a strong dependence on external magnetic field, confirming the precessional nature of the switching process. Moreover, it is seen that below the threshold field of around $B_{ext} = 90$ mT, switching does not occur at all. This emphasizes the role of the external field, being a necessary driving force for the precessional switching process.

Aiming to reveal how the oscillations depend on magnetic field, we plot the waveforms at the optimal fluence ($F = 1.1$ mJ cm^{-2}) for various external magnetic fields in Figure 6b. The linear dependence of the resonance frequency on external magnetic field with a characteristic slope of $\approx \gamma/2\pi = 28$ GHz T^{-1}, depicted in the inset, is in accordance with ferromagnetic resonance.[28–30] In this case, the net magnetization precesses around the "effective" magnetic field, $\boldsymbol{H}_{eff} = -\delta F/\delta \boldsymbol{M}$ derived from the appropriate free energy F.[1] From this, we can understand the fluence- and time-dependence of the frequency ω_{FM} from Figure 4, as the resonance frequency is fully determined by the total effective field. In our case, this field includes contributions of the external field H_{ext}, anisotropy field H_A (see Figure 1) as well as the demagnetizing field $\boldsymbol{H}_D$.[28,29] The latter contribution, also known as shape anisotropy, contributes like an easy-plane type of anisotropy, proportional to the net magnetization and thus being large far away from the compensation temperature.[31] However, given the fact that our measurements were performed near the magnetization compensation temperature, we argue that this contribution is small and can be ignored. As the external field remains constant during the experiment, only transient changes of the magnetic anisotropy $\omega_{FM}(H_{ext}, H_A(t))$ can be held responsible for the time- and fluence-dependencies of ω_{FM}. This conclusion will be a key ingredient for the theory of the coming section that describes the sub-ns magnetization dynamics.

4. Theory

Based on the fluence- and time-dependence of the observed resonance frequency ω_{FM} from Figure 4, we suggest that the observed effects must be a consequence of the thermal transient modification of the anisotropy field $H_A(T(t)) = [2K(T)M_z(T)/M(T)^2]\hat{\boldsymbol{z}}$. The modification of magnetic anisotropy strongly depends on the temperature-dependence of the uniaxial anisotropy constant $K(T)$, which in thermodynamic equilibrium usually follows the Callen–Callen power-law dependence with the magnetization[32]

$$\frac{K(T)}{K(0)} = \left[\frac{M(T)}{M(0)}\right]^n \tag{1}$$

Here n is a material-specific constant determined by the specific origin of the anisotropy.[33] Provided $n \neq 1$, this will result in a thermal modification of the anisotropy field $H_A(T)$ after laser-induced heating. The value of n was reported earlier in a rather broad range,[8,32–34] but for the case of uniaxial anisotropy n it is theoretically predicted to be $n = 3$.[35,36] Here, we will use this transient modification of anisotropy and show that it allows us to explain the experimentally observed phenomena.

4.1. Magnetization Reversal Based on LLB Formalism

To study the consequence of Equation (1) on the magnetization dynamics of our metallic multilayer, we follow the approach by Atxitia et al.,[37,38] using the stochastic Landau–Lifshitz–Bloch (LLB) equations to describe magnetization dynamics ferrimagnets. The corresponding equations are written in a compact form for the reduced magnetization vector $\boldsymbol{m}_v = \boldsymbol{M}_v/M_{v,0}$, with v = Gd, Fe:

$$\dot{\boldsymbol{m}}_v = -\gamma_v[\boldsymbol{m}_v \times \boldsymbol{H}_{eff,v}] - \gamma_v \alpha_\parallel^v \frac{(\boldsymbol{m}_v \cdot \boldsymbol{H}_{eff,v}^\parallel)}{m_v^2}\boldsymbol{m} - \gamma_v \alpha_\perp^v \frac{[\boldsymbol{m}_v \times [\boldsymbol{m}_v \times \boldsymbol{H}_{eff,v}]]}{m_v^2} \tag{2}$$

The exact expressions of the transverse and longitudinal effective fields $\boldsymbol{H}_{eff,v}$, $\boldsymbol{H}_{eff,v}^\parallel$, and damping parameters $\alpha_\perp^v$, $\alpha_\parallel^v$ can be found in Ref. [37]. The parameters such as the exchange coupling, anisotropy, and saturation magnetization were taken from Ref. [39], and were adjusted to obtain the experimentally observed $T_M = 320$ K. In particular, in order to account for weaker Gd-FeCo exchange interaction in Gd/FeCo multilayers in comparison with that in the corresponding GdFeCo alloy, we have increased the intra-sublattice exchange as compared to the inter-sublattice exchange. After this, we manually adapted the parameters to reproduce the correct magnetization

2201283 (5 of 9)

compensation point. This can be found in the Supporting Information, where we plot the simulated static temperature dependence of the magnetic sublattices.

Having calculated the equilibrium magnetization, we study the evolution of the system after laser-induced heating, which has been accurately described by the phenomenological four-temperature model where four heat reservoirs corresponding to the electrons, the lattice and the two spin sublattices are involved.[40,41] In a mean-field approach such as the stochastic LLB formalism, the concept of spin-temperature is not well-defined, and generally the electron temperature is modeled using the conventional two-temperature (2T) model[42] (described in the Supporting Information) that couples to the spin baths via a coupling parameter.[37,43,44] Modeling laser-matter interaction in terms of the 2T model, an ultrafast laser pulse first deposits its energy into the electronic system which then exchanges the heat with the lattice on a time-scale of the electron-phonon interaction (≈2 ps). Such a heating results in a demagnetization of both the Gd and FeCo sublattices and lifts the temperature above T_M, making the state with a reversed orientation of the spins favorable. However, our simulations show that solely this fact will not induce switching of the magnetization. The boundary to the reversed state that is determined by the magnetic anisotropy needs to be diminished, as illustrated in **Figure 7**a. This can be achieved by assuming a temperature dependent transient magnetic anisotropy described by Equation (1) using the value of $n = 3$ for uniaxial anisotropy.[35,36] Furthermore, we assume that the anisotropy is completely dominated by the Gd sublattice, as was claimed earlier in the case of RE-TM alloys and multilayers.[45–48] More specifically, this means we replace $M(T)$ by $M_{Gd}(T)$ in Equation (1) and let only $M_{Gd}(T)$ contribute to the anisotropy energy. The latter assumption, together with the Callen–Callen power law taking $n = 3$, will greatly reduce the anisotropy field barrier, providing the necessary "kick-start" to the precessional switching process.

In Figure 7b, we plot the resulting dynamics of the Gd and Fe sublattice magnetizations $m_{Gd}(t)$ and $m_{Fe}(t)$ separately, and obtain a result that is in qualitative agreement with our experimental data. Similar to the experimental result in Figure 6a, the simulated long time-scale magnetization reversal that occurs after a quick demagnetization shows a characteristic dependence on external magnetic field. Moreover, we also obtain a "threshold field" below which the switching does not take place. The simulations theoretically demonstrate how the temperature dependence of magnetic anisotropy can result in precessional switching, after the Gd/FeCo multilayer has been brought to a non-equilibrium state by laser-induced heating.

It should be noted that in the experiments, we measure Faraday rotation and not net magnetic moment. The contributions from $M_{Gd,z}$ and $M_{Fe,z}$ to the Faraday effect are in general unequal[20]

$$\theta_F(T,\lambda) = a_{Gd}(T,\lambda)M_{Gd,z}(T) - a_{Fe}(T,\lambda)M_{Fe,z}(T) \qquad (3)$$

where the $a_v(T, \lambda)$ are wavelength- and temperature-dependent material-specific magneto–optical parameters. It is known that these parameters could allow certain sublattices to dominate the magneto–optical effect for specific wavelengths.[49] In the case of GdFeCo alloys, it is conventionally accepted that the transition-
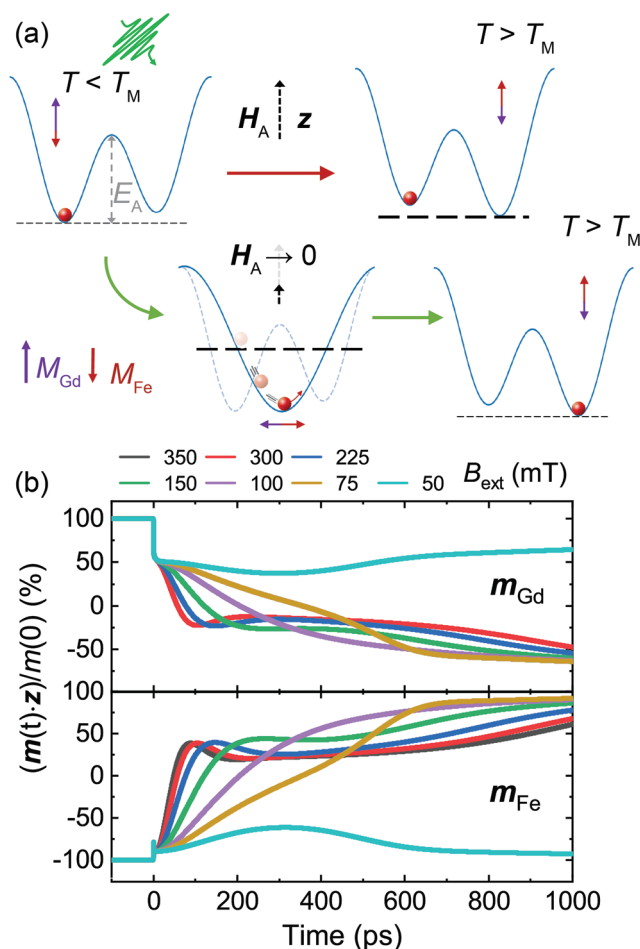

Figure 7. a) Schematic potential energy scheme of the reversal process. Initially when $T < T_M$, the free energy of the magnetic system is characterized by two potential minima corresponding to the stable Gd-dominated state and the meta-stable Fe-dominated state. In the simplest picture, the laser heats the system above the compensation temperature and makes the Fe-dominated state stable. However, the large barrier energy barrier E_A imposed by the anisotropy field H_A prevents switching to the new global minimum. By thermally leveraging the anisotropy field $H_A \rightarrow 0$, the barrier will be lifted and reversal may take place. b) Field-assisted double-step switching process as simulated by the LLB equations (Equation (2)) after laser-induced heating solved by the 2T model (for equations see Supporting Information), where we took the anisotropy field dynamics from M_{Gd} with $n = 3$ in Equation (1) into account. The parameters and mean-field equilibrium magnetizations used in the modelling are summarized in the Supporting Information.

metal is dominant at the wavelength of 800 nm. Contrary to this conventional wisdom, the simulated dynamics of the Gd sublattice shows a slightly better quantitative agreement to the experimental data than that of Fe (when comparing Figure 7b to Figure 6a). In the case of Gd/FeCo multilayers, it is strictly speaking unknown if FeCo dominates the magneto–optical signal, and our results suggest that Gd must be taken into account.

4.2. Large-Amplitude Precession Based on LLG Equation

Finally, we would like to return to the question of the unusually large precession amplitudes at low pump-fluences. As a

first simple attempt to describe this dynamics, we show that it can also be explained by considering the thermal modification of the anisotropy of a single macrospin. For this purpose, we consider the magnetization dynamics of a single magnetic moment M with initially $|M| \equiv M(0) = 0.2\mu_B$ described by the normalized Landau–Lifshitz–Gilbert (LLG) equation[29]

$$\frac{d\mathbf{m}}{dt} = -\gamma \mathbf{m} \times \mathbf{H}_{\text{eff}} + \alpha \left(\mathbf{m} \times \frac{d\mathbf{m}}{dt} \right) \tag{4}$$

Here $\mathbf{m}(t) = \mathbf{M}(t)/|\mathbf{M}(t)|$. We chose a Gilbert constant of $\alpha = 0.1$ and the effective field $\mathbf{H}_{\text{eff}} = \mathbf{H}_{\text{ext}} + \mathbf{H}_A$ is taken to include the external field $\mathbf{H}_{\text{ext}} = H(\cos\theta_H, 0, \sin\theta_H)$ and uniaxial anisotropy field $\mathbf{H}_A \equiv (2KM_z/M^2)\hat{\mathbf{z}}$.

We model the effect of ultrafast demagnetization by the double-exponential function[50]

$$|\mathbf{M}(t)|/M(0) = C\left[\exp(-t/\tau_1) - \exp(-t/\tau_2)\right] + 1 \tag{5}$$

where C sets the degree of demagnetization and $\tau_1 = 10$ ps, $\tau_2 = 1500$ ps define the timescales of demagnetization and relaxation, respectively. This demagnetization will result in a temperature dependence of the anisotropy field through $K(T)$ as in Equation (1) (again using $n = 3$), and the resulting modification of anisotropy $H_A(t)$ will be used as input for the normalized LLG Equation (4). The anisotropy field will be increasingly quenched for greater C, being almost completely zero for for a brief amount of time when $C = 1$ (see Supporting Information).

When simulating the effect of $H_A(t)$ on the transverse dynamics of $\mathbf{m}(t)$ for several values of C using the LLG Equation (4), we see in **Figure 8** that approaching nearly complete temporary quenching of anisotropy ($C = 1$) has a profound impact on the amplitude of the resulting precession, reaching the size of the magnetization vector itself. In order to make a translation of this simple model to our experimental results, one should note that even if the net magnetization is zero, it does not imply complete demagnetization of the individual magnetic
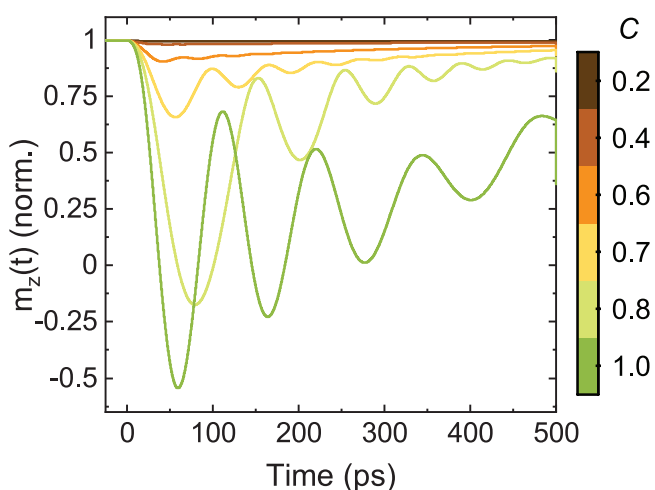
sublattices of a ferrimagnet. In fact, this is what occurs at the magnetization compensation point T_M. Given that our magnetization compensation point is only ≈30 K above room temperature, it could explain why we see the effect of full suppression of the anisotropy field already for low laser-fluences $0.3 \leqslant F \leqslant 1.6$ mJ cm^{-2} as in Figure 3. However, we should mention it is not necessarily the magnetization compensation temperature that matters. Analogue to the angular momentum compensation point, which is different from T_M when the contributions to the angular momentum from both sublattices are unequal, we should rather speak about the "anisotropy compensation temperature". Such a temperature could exist given that the anisotropy contributions from Fe and Gd are in general unequal. In the end, this simple model shows how the quenching of magnetic anisotropy can induce large-amplitude ferromagnetic resonance precession as observed in our experiment.

5. Conclusion

By extensive experimental and numerical analysis, we have been able to demonstrate the role of ultrafast modification of magnetic anisotropy in the laser-induced spin-dynamics of a Gd/FeCo multilayer. In the previous section, we explained the experimental results by considering the effect of thermal modification of a phenomenological uniaxial out-of-plane anisotropy field in the LLB and LLG formalisms. First, these results show that the ultrafast modification of magnetic anisotropy triggers magnetization reversal when the system is heated across the magnetization compensation point by an ultrafast laser pulse in the presence of an external magnetic field. This outcome shares many similarities with results obtained in YIG,[8] but requires a ≈100 times lower pulse-fluence. Second, we show that ultrafast quenching of the magnetic anisotropy could explain the unusually large magnetization precession. As the resonance frequency ω_{FM} itself is a function the anisotropy field, this means that the transient modification of anisotropy becomes directly evident in the time- and fluence-dependence of this frequency (see Figure 4). It was previously suggested that such a behavior of $\omega_{\text{FM}}(T(t))$ could be used to study the exact evolution of magnetic anisotropy after ultrafast laser excitation.[51]

We want to emphasize that the phenomenological theory is subjected to many simplifying assumptions and approximations, and that we did not consider microscopic details. In particular, we did not consider the (microscopic) origins of this anisotropy field, e.g., crystal-field effects, surface anisotropy etc., which all have different thermal dependencies, and which should be a subject of study for later research. But we can speculate that the main difference of the dynamics of Gd/FeCo multilayers with respect to the corresponding alloy is caused by symmetry-breaking at numerous interfaces of the magnetic multilayer. This is interesting from an engineering perspective, as controlling the number of interfaces and their degree of intermixing would therefore control the thermal gradient of the anisotropy and could serve as an additional degree of freedom when engineering materials suitable for field-assisted switching of magnetization. The degree of intermixing can for instance be controlled by Ga$^+$ irradiation of the multilayer,[15] or by sputtering conditions.

Figure 8. Result of LLG simulations using Equation (4) for several values of the parameter C from Equation (5). When $C = 1$ the anisotropy field touches $H_A = 0$ (see Supporting Information). This simple model shows that the thermal quenching of out-of-plane anisotropy has a large impact on the subsequent ferromagnetic resonance amplitude.

In general, our results fuel a renewed interest in the role and tunability of magnetic anisotropies in rare-earth transition-metal alloys and heterostructures,[51–53] as a result of the general ongoing fundamental and technological interest in the physics of ferrimagnets for spintronics applications.[54–57] The additional degree of freedom obtained using ultrafast modification of the magnetic anisotropy has not been extensively considered, and could lower the heat-threshold for reversing the magnetization without the loss of anisotropy and therefore stability of magnetic recording devices.

Supporting Information

Supporting Information is available from the Wiley Online Library or from the author.

Conflict of Interest

The authors declare no conflict of interest.

Data Availability Statement

The data that support the findings of this study are available from the corresponding author upon reasonable request.

[1] A. Kirilyuk, A. V. Kimel, T. Rasing, *Rev. Mod. Phys.* **2010**, *82*, 2731.
[2] C. D. Stanciu, F. Hansteen, A. V. Kimel, A. Kirilyuk, A. Tsukamoto, A. Itoh, T. Rasing, *Phys. Rev. Lett.* **2007**, *99*, 047601.
[3] I. Radu, K. Vahaplar, C. Stamm, T. Kachel, N. Pontius, H. A. Dürr, T. A. Ostler, J. Barker, R. F. L. Evans, R. W. Chantrell, A. Tsukamoto, A. Itoh, A. Kirilyuk, T. Rasing, A. V. Kimel, *Nature* **2011**, *472*, 205.
[4] T. A. Ostler, J. Barker, R. F. L. Evans, R. W. Chantrell, U. Atxitia, O. Chubykalo-Fesenko, S. El Moussaoui, L. Le Guyader, E. Mengotti, L. J. Heyderman, F. Nolting, A. Tsukamoto, A. Itoh, D. Afanasiev, B. A. Ivanov, A. M. Kalashnikova, K. Vahaplar, J. Mentink, A. Kirilyuk, T. Rasing, A. V. Kimel, *Nat. Commun.* **2012**, *3*, 666.
[5] A. Stupakiewicz, K. Szerenos, D. Afanasiev, A. Kirilyuk, A. Kimel, *Nature* **2017**, *542*, 71.
[6] M. H. Kryder, E. C. Gage, T. W. McDaniel, W. A. Challener, R. E. Rottmayer, G. Ju, Y.-T. Hsia, M. F. Erden, *Proc. IEEE* **2008**, *96*, 1810.
[7] W. A. Challener, C. Peng, A. V. Itagi, D. Karns, W. Peng, Y. Peng, X. Yang, X. Zhu, N. J. Gokemeijer, Y.-T. Hsia, G. Ju, R. E. Rottmayer, M. A. Seigler, E. C. Gage, *Nat. Photonics* **2009**, *3*, 220.
[8] C. S. Davies, K. H. Prabhakara, M. D. Davydova, K. A. Zvezdin, T. B. Shapaeva, S. Wang, A. K. Zvezdin, A. Kirilyuk, T. Rasing, A. V. Kimel, *Phys. Rev. Lett.* **2019**, *122*, 027202.
[9] S. Mangin, M. Gottwald, C.-H. Lambert, D. Steil, V. Uhlíř, L. Pang, M. Hehn, S. Alebrand, M. Cinchetti, G. Malinowski, Y. Fainman, M. Aeschlimann, E. E. Fullerton, *Nat. Mater.* **2014**, *13*, 286.
[10] M. S. E. Hadri, M. Hehn, G. Malinowski, S. Mangin, *J. Phys. D: Appl. Phys.* **2017**, *50*, 133002.
[11] M. L. M. Lalieu, M. J. G. Peeters, S. R. R. Haenen, R. Lavrijsen, B. Koopmans, *Phys. Rev. B* **2017**, *96*, 220411.
[12] M. Beens, M. L. M. Lalieu, A. J. M. Deenen, R. A. Duine, B. Koopmans, *Phys. Rev. B* **2019**, *100*, 220409.
[13] L. Avilés-Félix, A. Olivier, G. Li, C. S. Davies, L. Álvaro-Gómez, M. Rubio-Roy, S. Auffret, A. Kirilyuk, A. V. Kimel, T. Rasing, L. D. Buda-Prejbeanu, R. C. Sousa, B. Dieny, I. L. Prejbeanu, *Sci. Rep.* **2020**, *10*, 5211.
[14] U. Gradmann, *Appl. Phys.* **1974**, *3*, 161.
[15] M. C. H. de Jong, M. J. Meijer, J. Lucassen, J. van Liempt, H. J. M. Swagten, B. Koopmans, R. Lavrijsen, *Phys. Rev. B* **2022**, *105*, 064429.
[16] K. Vahaplar, A. M. Kalashnikova, A. V. Kimel, D. Hinzke, U. Nowak, R. Chantrell, A. Tsukamoto, A. Itoh, A. Kirilyuk, T. Rasing, *Phys. Rev. Lett.* **2009**, *103*, 117201.
[17] N. N. Greenwood, A. Earnshaw, *Chemistry of the Elements*, Elsevier, Oxford **1997**.
[18] R. C. Weast, *Handbook of Chemistry and Physics*, 53rd ed., Chemical Rubber Publisher, Cleveland **1972**.
[19] L. D. Landau, E. Lifshitz, *Phys. Z. Sowjet.* **1935**, *8*, 153.
[20] A. K. Zvezdin, V. A. Kotov, *Modern Magnetooptical Materials*, IOP Publishing, London **1997**.
[21] B. Koopmans, M. van Kampen, J. T. Kohlhepp, W. J. M. de Jonge, *Phys. Rev. Lett.* **2000**, *85*, 844.
[22] P. S. Pershan, *Phys. Rev.* **1963**, *130*, 919.
[23] E. Beaurepaire, J.-C. Merle, A. Daunois, J.-Y. Bigot, *Phys. Rev. Lett.* **1996**, *76*, 4250.
[24] R. Medapalli, I. Razdolski, M. Savoini, A. R. Khorsand, A. Kirilyuk, A. V. Kimel, T. Rasing, A. M. Kalashnikova, A. Tsukamoto, A. Itoh, *Phys. Rev. B* **2012**, *86*, 054442.
[25] A. Tsukamoto, T. Sato, S. Toriumi, A. Itoh, *J. Appl. Phys.* **2011**, *109*, 07D302.
[26] R. R. Subkhangulov, H. Munekata, T. Rasing, A. V. Kimel, *Phys. Rev. B* **2014**, *89*, 060402.
[27] S. Baierl, M. Hohenleutner, T. Kampfrath, A. Zvezdin, A. V. Kimel, R. Huber, R. Mikhaylovskiy, *Nat. Photonics* **2016**, *10*, 715.
[28] C. Kittel, *J. Phys. Radium* **1951**, *12*, 291.
[29] A. G. Gurevich, G. A. Melkov, *Magnetization Oscillations and Waves*, CRC Press, London **1996**.
[30] C. D. Stanciu, A. V. Kimel, F. Hansteen, A. Tsukamoto, A. Itoh, A. Kirilyuk, T. Rasing, *Phys. Rev. B* **2006**, *73*, 220402.
[31] J. M. D. Coey, *Magnetism and Magnetic Materials*, Cambridge University Press, Cambridge **2010**.
[32] H. Callen, E. Callen, *J. Phys. Chem. Solids* **1966**, *27*, 1271.
[33] B. K. Chatterjee, C. K. Ghosh, K. K. Chattopadhyay, *J. Appl. Phys.* **2014**, *116*, 153904.

[34] J.-Y. Bigot, M. Vomir, L. Andrade, E. Beaurepaire, *Chem. Phys.* **2005**, *318*, 137.

[35] J. H. van Vleck, *Phys. Rev.* **1937**, *52*, 1178.

[36] C. Zener, *Phys. Rev.* **1954**, *96*, 1335.

[37] U. Atxitia, P. Nieves, O. Chubykalo-Fesenko, *Phys. Rev. B* **2012**, *86*, 104414.

[38] U. Atxitia, T. Ostler, J. Barker, R. F. L. Evans, R. W. Chantrell, O. Chubykalo-Fesenko, *Phys. Rev. B* **2013**, *87*, 224417.

[39] T. A. Ostler, R. F. L. Evans, R. W. Chantrell, U. Atxitia, O. Chubykalo-Fesenko, I. Radu, R. Abrudan, F. Radu, A. Tsukamoto, A. Itoh, A. Kirilyuk, T. Rasing, A. Kimel, *Phys. Rev. B* **2011**, *84*, 024407.

[40] A. J. Schellekens, B. Koopmans, *Phys. Rev. B* **2013**, *87*, 020407.

[41] A. Mekonnen, A. R. Khorsand, M. Cormier, A. V. Kimel, A. Kirilyuk, A. Hrabec, L. Ranno, A. Tsukamoto, A. Itoh, T. Rasing, *Phys. Rev. B* **2013**, *87*, 180406.

[42] J. Chen, D. Tzou, J. Beraun, *Int. J. Heat Mass Transfer* **2006**, *49*, 307.

[43] U. Atxitia, T. A. Ostler, R. W. Chantrell, O. Chubykalo-Fesenko, *Appl. Phys. Lett.* **2015**, *107*, 192402.

[44] C. Davies, T. Janssen, J. Mentink, A. Tsukamoto, A. Kimel, A. van der Meer, A. Stupakiewicz, A. Kirilyuk, *Phys. Rev. Appl.* **2020**, *13*, 024064.

[45] M. D. Davydova, K. A. Zvezdin, J. Becker, A. V. Kimel, A. K. Zvezdin, *Phys. Rev. B* **2019**, *100*, 064409.

[46] M. Davydova, P. Skirdkov, K. Zvezdin, J.-C. Wu, S.-Z. Ciou, Y.-R. Chiou, L.-X. Ye, T.-H. Wu, R. C. Bhatt, A. Kimel, A. Zvezdin, *Phys. Rev. Appl.* **2020**, *13*, 034053.

[47] J. Becker, A. Tsukamoto, A. Kirilyuk, J. C. Maan, T. Rasing, P. C. M. Christianen, A. V. Kimel, *Phys. Rev. Lett.* **2017**, *118*, 117203.

[48] A. Pogrebna, K. Prabhakara, M. Davydova, J. Becker, A. Tsukamoto, T. Rasing, A. Kirilyuk, A. K. Zvezdin, P. C. M. Christianen, A. Kimel, *Phys. Rev. B* **2019**, *100*, 174427.

[49] A. R. Khorsand, M. Savoini, A. Kirilyuk, A. V. Kimel, A. Tsukamoto, A. Itoh, T. Rasing, *Phys. Rev. Lett.* **2013**, *110*, 107205.

[50] R. F. L. Evans, T. A. Ostler, R. W. Chantrell, I. Radu, T. Rasing, *Appl. Phys. Lett.* **2014**, *104*, 082410.

[51] P. I. Gerevenkov, D. V. Kuntu, I. A. Filatov, L. A. Shelukhin, M. Wang, D. P. Pattnaik, A. W. Rushforth, A. M. Kalashnikova, N. E. Khokhlov, *Phys. Rev. Mater.* **2021**, *5*, 094407.

[52] N. O. Antropov, E. A. Kravtsov, M. V. Makarova, V. V. Proglyado, T. Keller, I. A. Subbotin, E. M. Pashaev, G. V. Prutskov, A. L. Vasiliev, Y. M. Chesnokov, N. G. Bebenin, M. A. Milyaev, V. V. Ustinov, B. Keimer, Y. N. Khaydukov, *Phys. Rev. B* **2021**, *104*, 054414.

[53] A. Chanda, J. E. Shoup, N. Schulz, D. A. Arena, H. Srikanth, *Phys. Rev. B* **2021**, *104*, 094404.

[54] J. Barker, U. Atxitia, *J. Phys. Soc. Jpn.* **2021**, *90*, 081001.

[55] S. Iihama, Q. Remy, J. Igarashi, G. Malinowski, M. Hehn, S. Mangin, *J. Phys. Soc. Jpn.* **2021**, *90*, 081009.

[56] S. K. Kim, G. S. Beach, K.-J. Lee, T. Ono, T. Rasing, H. Yang, *Nat. Mater.* **2022**, *21*, 24.

[57] A. Kirilyuk, A. V. Kimel, T. Rasing, *Rep. Prog. Phys.* **2013**, *76*, 026501.

[58] J. Barker, U. Atxitia, T. A. Ostler, O. Hovorka, O. Chubykalo-Fesenko, R. W. Chantrell, *Sci. Rep.* **2013**, *3*, 3262.

[59] P. E. Hopkins, M. Ding, J. Poon, *J. Appl. Phys.* **2012**, *111*, 103533.

[60] K. Vahaplar, Ph.D. thesis, Radboud University Nijmegen **2011**.

2201283 (9 of 9)